Neuron
Article

Aberrant Schwann Cell Lipid Metabolism Linked to Mitochondrial Deficits Leads to Axon Degeneration and Neuropathy

Andreu Viader,[1] Yo Sasaki,[1] Sungsu Kim,[1] Amy Strickland,[1] Cayce S. Workman,[1] Kui Yang,[2] Richard W. Gross,[2] and Jeffrey Milbrandt[1,3,*]
[1]Department of Genetics
[2]Division of Bioorganic Chemistry and Molecular Pharmacology, Department of Internal Medicine
[3]Hope Center for Neurological Diseases
Washington University School of Medicine, St. Louis, MO 63110, USA
*Correspondence: jmilbrandt@wustl.edu
http://dx.doi.org/10.1016/j.neuron.2013.01.012

SUMMARY

Mitochondrial dysfunction is a common cause of peripheral neuropathy. Much effort has been devoted to examining the role played by neuronal/axonal mitochondria, but how mitochondrial deficits in peripheral nerve glia (Schwann cells [SCs]) contribute to peripheral nerve diseases remains unclear. Here, we investigate a mouse model of peripheral neuropathy secondary to SC mitochondrial dysfunction (Tfam-SCKOs). We show that disruption of SC mitochondria activates a maladaptive integrated stress response (ISR) through the actions of heme-regulated inhibitor (HRI) kinase, and causes a shift in lipid metabolism away from fatty acid synthesis toward oxidation. These alterations in SC lipid metabolism result in depletion of important myelin lipid components as well as in accumulation of acylcarnitines (ACs), an intermediate of fatty acid β-oxidation. Importantly, we show that ACs are released from SCs and induce axonal degeneration. A maladaptive ISR as well as altered SC lipid metabolism are thus underlying pathological mechanisms in mitochondria-related peripheral neuropathies.

INTRODUCTION

Mitochondrial metabolic irregularities are a common culprit in diverse neurodegenerative diseases and are key pathological contributors to peripheral neuropathy. Mitochondrial dysfunction is thought to be largely responsible for the peripheral nerve deficits that afflict large numbers of people with diabetes and can lead to incapacitating pain, sensory loss, and debilitating muscle weakness (Fernyhough et al., 2010). Similarly, a number of mutations in mitochondrial proteins have now been identified as the cause of several forms of inherited neuropathies known as Charcot-Marie-Tooth (CMT) (Niemann et al., 2006). The need to elucidate the manner in which mitochondrial dysfunction underlies the progression of peripheral nerve disease is thus well appreciated, and to date, much effort has been devoted to clarifying the role played by neuronal/axonal mitochondria in peripheral neuropathies (Baloh, 2008).

Glial cells, however, are involved in virtually every aspect of nervous system function (Barres, 2008). Hence, it is increasingly being recognized that glia influence neurodegenerative diseases that were traditionally thought to be neuron autonomous (e.g., amyotrophic lateral sclerosis; Ilieva et al., 2009). In the peripheral nervous system, glial cells known as Schwann cells (SCs) critically support the long-term preservation and function of all peripheral nerve axons, as well as their repair after damage (Nave and Trapp, 2008). Interestingly, abnormal mitochondria in the nerves of patients with neuropathy often localize to SCs (Schröder, 1993; Kalichman et al., 1998). Mitochondrial dysfunction specifically in SCs is thus likely to be a critical mediator of nerve pathology, and understanding how mitochondrial deficits in these glia contribute to disease progression could facilitate development of novel treatments for peripheral neuropathies.

To directly interrogate the contribution of SC mitochondrial dysfunction to peripheral nerve disease, we recently generated mice (Tfam-SCKOs) with disrupted mitochondrial metabolism exclusively in SCs (Viader et al., 2011). Remarkably, these mice recapitulated key pathological features of human neuropathies, making them a valuable model in which to examine the pathological processes that drive mitochondrial peripheral nerve disorders. In the present work, we use this model of neuropathy to demonstrate that SC mitochondrial dysfunction contributes to disease progression by activating a maladaptive integrated stress response (ISR) through the actions of heme-regulated inhibitor (HRI) kinase. Moreover, we also identify a mitochondrial-dysfunction-induced shift in SC lipid metabolism away from new lipid synthesis toward increased fatty acid oxidation. This metabolic alteration results in early depletion of myelin lipid components as well as a large accumulation of acylcarnitine (AC) lipid intermediates. Importantly, we show that ACs are released from SCs and induce axonal degeneration. Activation of a maladaptive ISR and altered SC lipid metabolism resulting in toxic accumulation of lipid intermediates are thus underlying mechanisms of axonal degeneration and demyelination in mitochondrial peripheral neuropathies and constitute potentially important therapeutic targets.

RESULTS

Tfam-SCKO Mice: A Model of Peripheral Neuropathy Secondary to SC Mitochondrial Dysfunction

With the goal of understanding whether SC mitochondrial abnormalities affect axonal survival and contribute to peripheral nerve diseases, we used the tissue-specific deletion of the mitochondrial transcription factor A gene (*Tfam*) to generate mice with impaired mitochondrial metabolism exclusively in SCs (Tfam-SCKOs; Viader et al., 2011). TFAM is a nuclear-encoded mitochondrial protein that is essential for the maintenance, transcription, and replication of mitochondrial DNA (mtDNA; Larsson et al., 1998; Ekstrand et al., 2004). Given that the mitochondrial genome encodes 13 subunits that are necessary components of complexes I, III, IV, and V of the electron transport chain, excision of *Tfam* from a tissue of interest results in severe mtDNA depletion and mitochondrial respiratory chain deficiency (Larsson et al., 1998; Silva et al., 2000; Viader et al., 2011). This makes the tissue-specific deletion of Tfam an effective way to induce mitochondrial dysfunction in a selected population of cells.

As detailed elsewhere (Viader et al., 2011), we achieved highly selective and efficient excision of *Tfam* from SCs by mating mice with *loxP*-flanked *Tfam* alleles ($Tfam^{loxP}$; Larsson et al., 1998) to mice that express *cre*-recombinase in both myelinating and nonmyelinating SCs via the myelin protein zero (P_0) promoter (Feltri et al., 1999). Following the SC-specific deletion of Tfam, and consistent with the essential role of this protein in the replication/transcription of mtDNA (Larsson et al., 1998; Ekstrand et al., 2004), we observed severe depletion of mtDNA and the transcripts it encodes (e.g., *mt-ND2* and *mt-Cox1*) in 2-month-old Tfam-SCKO nerves compared with controls (Figure S1A available online; Viader et al., 2011). This depletion resulted in the inhibition of mitochondrial respiratory chain enzymes and overall mitochondrial respiration in the nerves of Tfam-SCKO mice (Figures S1B and S1C; Viader et al., 2011). Accordingly, COX enzymatic staining, which reflects respiratory chain activity in individual cells, showed reduced staining intensity in the cell bodies of SCs in Tfam-SCKO sciatic nerves (Figure S1D). Moreover, electron microscopic examination of Tfam-SCKO nerves revealed many morphologically abnormal mitochondria in SCs as early as 1 month of age (Figure S1E; Viader et al., 2011), thus confirming that SC-specific deletion of Tfam resulted in mice with disrupted mitochondrial metabolism in peripheral nerve glia.

Interestingly, induction of SC-specific mitochondrial dysfunction did not affect SC survival (Viader et al., 2011). SC-specific mitochondrial deficits instead resulted in a severe, progressive peripheral neuropathy characterized by extensive axonal degeneration that recapitulated critical features of human neuropathy. As previously reported for polyneuropathies associated with diabetes (Kennedy et al., 1996), Tfam-SCKO nerves displayed early abnormalities and preferential loss of small unmyelinated C fibers (starting at 1–2 months of age; Figure 1A; Viader et al., 2011). This was followed by the degeneration of large-caliber myelinated axons (starting at 3–4 months of age; Figures 1B and 1C; Viader et al., 2011). Extensive demyelination was apparent at late stages of the disease (Figure 1B). Consistent with this nerve pathology, Tfam-SCKO mice developed progressive distal weakness and sensory deficits (Viader et al., 2011), which are common symptoms in patients with peripheral neuropathy. Therefore, Tfam-SCKO mice are a SC-specific metabolic mutant that recapitulates pathological aspects of human peripheral neuropathies.

Energy Depletion Does Not Drive Nerve Pathology in Tfam-SCKO Mice

Having established the utility of the Tfam-SCKO mouse model for understanding and potentially treating peripheral neuropathies, we explored causal mechanisms of the nerve pathology in these mice. Importantly, we focused our analysis on 2-month-old Tfam-SCKOs. At this age, SC mitochondrial function is already disrupted (Figures S1A–S1E), yet Tfam-SCKO nerves display only very limited, early pathological changes that are largely confined to unmyelinated fibers (Figures 1A–1C; Viader et al., 2011). By using pre-/early-pathological Tfam-SCKO mice, we ensured that the disease mechanisms we identified were drivers of subsequent nerve abnormalities rather than simply a reflection of them. All experiments described below were carried out on 2-month-old Tfam-SCKO mice in the early (prepathological) stage of the disorder.

We first determined the energy status of Ctrl and Tfam-deficient SCs because clinical deficits in diseases associated with mitochondrial dysfunction are often assumed to be directly related to depletion of cellular energy levels. Surprisingly, measurement of nerve adenylate pools and determination of the adenylate energy charge (EC), an index used to measure cellular energy status (see Experimental Procedures; Atkinson, 1968), revealed only a very slight energy reduction (≈8%) in Tfam-SCKO nerves (Ctrl, EC = 0.812 ± 0.009; Tfam-SCKO, EC = 0.747 ± 0.008; $p < 0.001$; Figure 1D). Increased mitochondrial content and glycolytic activity in Tfam-deficient SCs (Figures S1F–S1H), two metabolic adaptations that often follow mitochondrial deficits, likely account for the relative preservation of energy levels in Tfam-SCKO nerves.

To further examine the energy status of Tfam-deficient SCs, we next assessed the phosphorylation of the cellular energy sensor AMP-activated protein kinase (AMPK). Phosphorylation at Thr172 activates AMPK and is induced by increases in the cellular AMP:ATP ratio (Hardie et al., 2012), making it a good indicator of reductions in cellular energy levels. We observed no difference in the level of AMPK phosphorylation between 2-month-old Ctrl and Tfam-SCKO nerves (Figure 1E). Together, these results indicate that Tfam-deficient SCs do not experience energy depletion to an extent that is likely to be responsible for the nerve pathology observed in these mice.

Mitochondrial Dysfunction in SCs Activates a Maladaptive ISR

In an attempt to identify other potential disease-causing processes, we carried out gene-expression profiling of 2-month-old Ctrl and Tfam-SCKO nerves. This analysis uncovered the upregulation of a number of genes activated by the ISR (e.g., *Ddit3/Chop*, *Asns*, *Mthfd2*, and *Trib3*) in SCs with disrupted mitochondrial metabolism (Table S1). The ISR is a conserved gene-expression program that helps cells withstand diverse

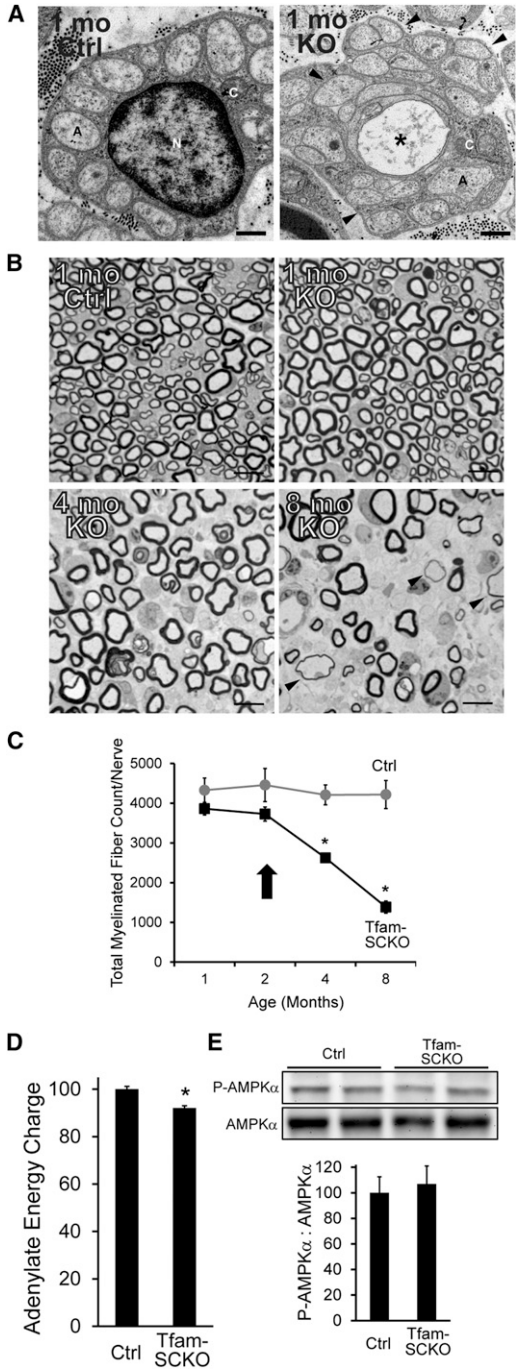

Figure 1. SC Mitochondrial Dysfunction Induces a Progressive, Degenerative Peripheral Neuropathy that Is Not Directly Linked to Energy Depletion

(A) Electron micrographs of 1-month-old Ctrl and Tfam-SCKO sciatic nerve cross-sections depicting early structural abnormalities of Remak bundles (SC surrounding multiple unmyelinated axons; arrowheads) and degeneration of unmyelinated axons (asterisk). A, axon; C, SC cytoplasm; N, SC nucleus. Scale bar, 500 nm.

(B and C) Toluidine-blue-stained plastic sections of Tfam-SCKO and Ctrl sciatic nerve cross-sections (B) and quantification of the total number of myelinated profiles per nerve (C) at different ages show prominent, progressive degeneration of large-caliber myelinated axons and demyelination starting at 3–4 months of age. Arrowheads (B) indicate axons surrounded by unusually thin myelin, a sign of demyelination. Arrow in (C) indicates the point in the progression of the pathology for all mice used in later experiments; note that at this age, nerves display only limited, early pathological changes with minimal axon loss and demyelination. N = 4 mice per genotype at each age. Error bars represent SEM; *$p < 0.01$. Scale bar, 25 μm.

(D) EC in 2-month-old Tfam-SCKO nerves shows only a slight decrease in the energy levels of Tfam-deficient SCs compared with Ctrl nerves. N = 8 mice per genotype. Error bars represent SEM; *$p < 0.01$. See also Figure S1.

(E) Immunoblot analysis and quantification of band intensity reveals no increase in the phosphorylation (activation) of the energy sensor AMPK in 2-month-old Tfam-SCKO nerves, indicating that energy depletion is an unlikely driver of nerve pathology in these mice. N = 4 mice per genotype. Error bars represent SEM. See also Figure S1.

cellular stresses by attenuating the rate of protein translation through the phosphorylation of the translation initiation factor 2α (eIF2α; Dalton et al., 2012). Importantly, previous work examining neuropathy models induced by mutations in structural myelin proteins showed that activation of the ISR is particularly maladaptive to SCs and can cause nerve pathology (Pennuto et al., 2008). This suggests that the ISR is a likely driver of disease progression in Tfam-SCKO mice, which prompted us to examine the activation of this pathway in more detail.

We confirmed ISR activation in 2-month-old Tfam-SCKOs nerves by verifying the upregulation of ISR target genes using quantitative RT-PCR (qRT-PCR; Figure 2A). Western blot analysis also showed hyperphosphorylation of eIF2α in Tfam-SCKO nerves compared with controls (Figure 2B). Moreover, we found that pharmacological inhibition of mitochondria in cultured SCs (e.g., using CCCP, antimycin, or oligomycin) also led to induction of ISR target genes (Figure 2C) and increased phosphorylation of eIF2α (Figure 2D). The maladaptive activation of the ISR downstream of eIF2α phosphorylation in Tfam-SCKO nerves is thus a primary effect of mitochondrial dysfunction in SCs.

Mitochondrial Dysfunction-Induced ISR Activation in SCs Is Mediated by HRI and Is Independent of ER Stress

In models of human neuropathy induced by mutations in myelin proteins, ISR activation is associated with endoplasmic reticulum (ER) stress or an unfolded protein response (UPR; Pennuto et al., 2008). Thus, we next sought to determine whether similar mechanisms were responsible for induction of the ISR in Tfam-SCKO nerves following respiratory chain deficiency. We found, however, that PKR-like ER kinase (PERK), the primary ER-stress sensor for ISR induction (Walter and Ron, 2011), was not activated in 2-month-old Tfam-SCKO nerves (as determined by its phosphorylation; Figure 3A). In agreement with this, expression of the UPR-induced molecular chaperon BiP/Grp78 was also not elevated in Tfam-SCKO nerves (Figure 3A). IRE-1, a second ER-stress sensor normally activated by the UPR (Walter and Ron, 2011), was also not engaged in either Tfam-SCKO nerves or cultured SCs treated with mitochondrial inhibitors (as determined by splicing of the IRE-1 target Xbp-1; Figure 3B). Therefore, mitochondrial electron transport chain deficits in SCs activate ISR through a process that is distinct from its activation by ER stress.

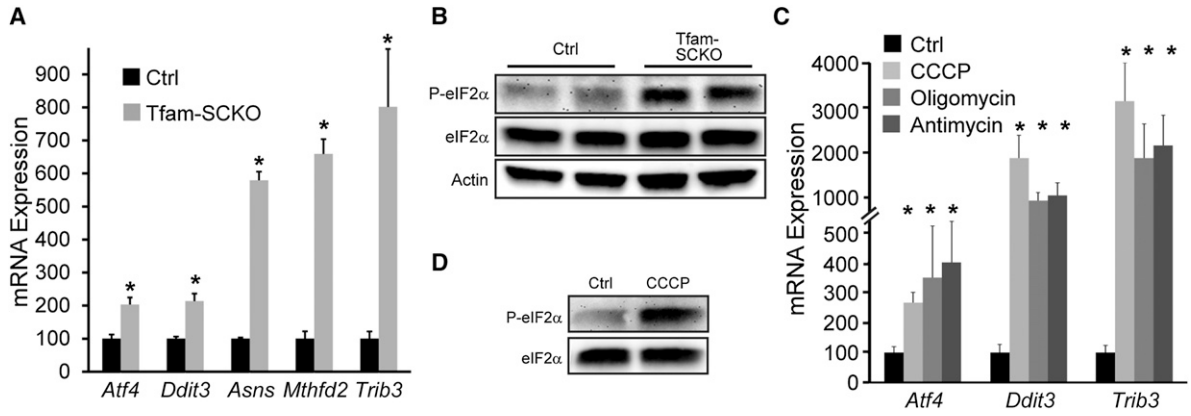

Figure 2. SC Mitochondrial Dysfunction Activates a Maladaptive ISR

(A) SC mitochondrial dysfunction upregulates the expression of ISR target genes in 2-month-old Tfam-SCKO nerves compared with Ctrl as measured by qRT-PCR. *Atf4*, activating transcription factor 4; *Ddit3*, DNA-damage inducible transcript 3; *Asns*, asparagine synthetase; *Mthfd2*, methylenetetrahydrofolate dehydrogenase; *Trib3*, tribbles homolog 3. N = 5 mice per genotype. Error bars represent SEM; *p < 0.05.

(B) Immunoblot analysis shows increased phosphorylation of eIF2α in 2-month-old Tfam-SCKO versus Ctrl nerves, confirming the activation of the ISR.

(C) Inhibition of mitochondrial respiration in cultured SCs with mitochondrial inhibitors upregulates the expression of ISR target genes as measured by qRT-PCR. N = duplicate wells from three independent experiments. Error bars represent SEM; *p < 0.05.

(D) Immunoblot analysis shows that application of the mitochondrial inhibitor CCCP to cultured SCs increases phosphorylation of eIF2α, indicating that inhibition of the mitochondrial electron transport chain activates the ISR.

See also Table S1.

Having excluded a role for PERK in the phosphorylation of eIF2α and downstream ISR activation in Tfam-SCKO mice, we attempted to identify the kinase responsible for these processes following mitochondrial dysfunction. We focused on general control nondepressible-2 kinase (GCN2), protein kinase RNA-activated (PKR), and HRI, three additional kinases that induce eIF2α phosphorylation in response to amino acid deprivation, viral infection, or iron deficiency, respectively (Dalton et al., 2012). We found that only knockdown of HRI was sufficient to prevent eIF2α phosphorylation in cultured cells following treatment with the mitochondrial inhibitor CCCP (Figures 3C and 3E). Accordingly, the subsequent eIF2α phosphorylation-dependent induction of the ISR mediator DDIT3/Chop was also prevented by HRI knockdown (Figure 3E). HRI activity is traditionally thought to be triggered by iron deficiency (Dalton et al., 2012), and our observations now link the kinase activity of HRI to defects in mitochondrial respiration. The maladaptive activation of the ISR in SCs through distinct eIF2α kinases that respond to diverse stressors (e.g., HRI to mitochondrial dysfunction, and PERK to ER stress) may thus be a central pathological mechanism common to multiple types of peripheral neuropathy.

Mitochondrial Dysfunction Alters SC Lipid Metabolism Homeostasis

The diverse etiology of mitochondrial neuropathies modeled by Tfam-SCKO mice is consistent with the notion that the interactions of multiple pathological processes ultimately drive disease progression. Therefore, we mined genes differentially expressed in 2-month-old Tfam-SCKO nerves to search for additional disease-causing processes. Interestingly, we found that lipid-related metabolic pathways were overrepresented in this set of genes (Figure 4A), suggesting alterations in SC lipid metabolism secondary to mitochondrial derangements. Indeed, qRT-PCR confirmed that a number of genes that are critically involved in lipid synthesis were downregulated in Tfam-deficient SCs, including fatty acid synthase (*Fasn*) and 3-hydroxy-3-methyl-glutaryl-coenzyme A (CoA) reductase (*Hmgcr*; Figure 4B). Moreover, we found that acetyl-CoA carboxylase (ACC) phosphorylation, which inhibits the activity of this enzyme (Figure 4C), was increased 3-fold in 2-month-old Tfam-SCKO nerves (Figures 4D and 4E). ACC supplies malonyl-CoA, which is required for lipid biosynthesis, thereby regulating the balance between lipid synthesis and oxidation (Figure 4C; Barber et al., 2005). Increased phosphorylation of ACC in Tfam-SCKO nerves and decreased expression of lipid synthetic genes are consistent with a shift in lipid metabolism away from new lipid synthesis and toward increased lipid oxidation. Given the central role of lipids in the normal biology of SCs (e.g., myelin formation; Chrast et al., 2011), this remodeling of SC lipid metabolism following mitochondrial deficits could be a second disease-causing process that is central to the pathology of Tfam-SCKO mice.

Mitochondrial Dysfunction-Induced Remodeling of SC Lipid Metabolism Depletes Key Myelin Lipid Components and Disrupts Axon–SC Interactions

To examine in more detail the implications of mitochondrial dysfunction-induced lipid changes for the pathology observed in Tfam-SCKO nerves, we performed a comprehensive analysis of the lipid composition of 2-month-old Ctrl and Tfam-SCKO nerves using multidimensional mass-spectrometry-based shotgun lipidomics (Yang et al., 2009). Among all the different lipid classes examined, cerebrosides (CBs) and sulfatides (STs) were the only lipid classes with reduced levels (30% and 40% reductions, respectively) in 2-month-old Tfam-SCKO nerves (Figures 5A and 5B). In peripheral nerves, CBs and STs are almost exclusively produced by SCs and are particularly

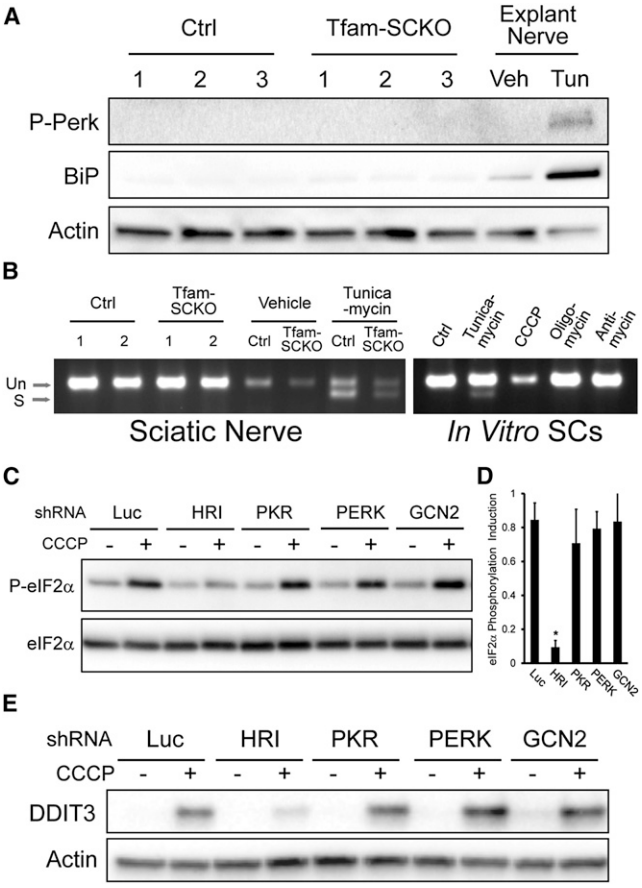

Figure 3. Mitochondrial Dysfunction-Induced ISR Activation in SCs Is Mediated by HRI Kinase Independently of ER Stress

(A) Immunoblot analysis of the phosphorylation (activation) status of the ER-stress sensor PERK and the UPR-induced molecular chaperone BiP/Grp78 in 2-month-old Ctrl and Tfam-SCKO nerves (three separate mice per genotype) shows no differences, indicating that ISR activation following SC mitochondrial deficits does not involve ER stress. Tunicamycin treatment of sciatic nerves cultured as explants serves as a positive control for ER stress. Tun, tunicamycin; Veh, vehicle.

(B) Gel showing the absence of Xbp-1 splicing downstream of the activation of the ER-stress sensor Ire-1 in 2-month-old Tfam-SCKO nerves, or SCs treated with mitochondrial inhibitors, confirms that ISR activation induced by mitochondrial derangement is independent of ER stress. Tunicamycin treatment of cultured SCs or sciatic nerves cultured as explants serves as a positive control for ER stress.

(C) Immunoblot analysis of eIF2α phosphorylation in 3T3 cells expressing shRNA to the indicated eIF2α kinases (HRI, PKR, PERK, and GCN2) that were treated for 3 hr with 5 μM CCCP to inhibit mitochondrial respiration. Knockdown of HRI (but not of GCN2, PKR, or PERK) is sufficient to prevent eIF2α phosphorylation following inhibition of mitochondrial respiration, indicating the specific role of HRI in this process.

(D) Quantification of the immunoblot as shown in (C) by densitometry. N = 3 independent experiments. Error bars represent SEM; *p < 0.05.

(E) Immunoblot analysis of the induction the ISR mediator DDIT3/CHOP 6 hr after inhibition of mitochondrial respiration with 5 μM CCCP in 3T3 cells in which expression of the indicated eIF2a kinase (HRI, PKR, PERK, or GCN2) was knocked down using shRNA. Knockdown of HRI (but not of GCN2, PKR, or PERK) is sufficient to prevent DDIT3/CHOP induction downstream of eIF2α phosphorylation following inhibition of mitochondrial respiration.

enriched in myelin; together they represent almost 30% of all lipid content in peripheral myelin (Garbay et al., 2000). The depletion of these two important myelin glycosphingolipids from Tfam-SCKO nerves is therefore in agreement with our observations suggesting that mitochondrial dysfunction in SCs results in a metabolic shift away from lipid biosynthesis.

Of importance for the pathology of Tfam-SCKO mice, ST and CB depletion disrupts saltatory conduction of action potentials and interferes with the maintenance of SC–axon contacts and ion channel clustering around the nodes of Ranvier (Dupree et al., 1998; Hoshi et al., 2007). In agreement with these reports, immunostaining of 2-month-old Tfam-SCKO nerves showed normal nodal clustering of voltage-gated sodium channels (Nav1.6; Figure 5C) but aberrant localization or loss of voltage-gated potassium channel clusters (Kv1.2) in the juxtaparanodal axolemma (Figures 5D and 5E). This abnormal clustering of ion channels is likely responsible for the reduced nerve conduction velocity (NCV) in 2-month-old Tfam-SCKO mice (NCV m/s, Ctrl = 24 ± 0.7, Tfam-SCKO = 15.7 ± 0.7; $p < 0.05$) and is indicative of disrupted axon–SC interactions. In fact, electron microscopic analysis of 2-month-old Tfam-SCKO nerves revealed enlarged nodal gaps (Figure 5F) as well as a significant number of axons that appeared to have pulled away from their myelin ensheathments (Figure 5G), both of which reflect abnormal axon–glia contacts. Similar structural abnormalities were not present in 1-month-old Tfam-SCKO mice (Figures S2C–S2E) in which nerve ST and CB content was still equivalent to that of Ctrl mice (Figures S2A and S2B).

Besides disrupting axon–SC interactions, the reduction of myelin lipid components induced by mitochondrial dysfunction may also contribute to the prominent demyelinating phenotype apparent in late stages of the disease (at >4 months of age) in Tfam-SCKO mice (Figure 1B; Viader et al., 2011). This is supported by the observation that depletion of STs and CBs preceded extensive demyelination (g-ratio at 2 months of age, axon area/fiber, Ctrl = 0.645 ± 0.008, Tfam-SCKO = 0.647 ± 0.006; Figures 1B and 1C) or changes in expression of myelin proteins (e.g., myelin basic protein [MBP]) in 2-month-old Tfam-SCKO nerves (Figures 5H and 5I). Depletion of myelin lipid components following respiratory-chain-deficiency-induced remodeling of SC lipid metabolism is thus a key driver of pathology in mitochondrial neuropathies.

Accumulation of Toxic Lipid Oxidation Intermediates Characterizes the Mitochondrial-Dysfunction-Induced Remodeling of SC Lipid Metabolism

The most prominent alteration in lipid composition in 2-month-old Tfam-SCKO nerves, however, was a 25-fold increase in AC species (Figure 6A). This increase affected most long-chain ACs, with the levels of some species being hundreds of times higher in Tfam-SCKO than in Ctrl nerves (Figures 6B, S3C, and S3D). ACs are intermediates in transporting fatty acyl groups across the mitochondrial membrane, which is required for these groups to undergo fatty acid β-oxidation, an important source of cellular energy and anabolic metabolites (Figure 6C; Houten and Wanders, 2010). Increased AC levels in Tfam-SCKO nerves, therefore, support our previous observations suggesting a shift

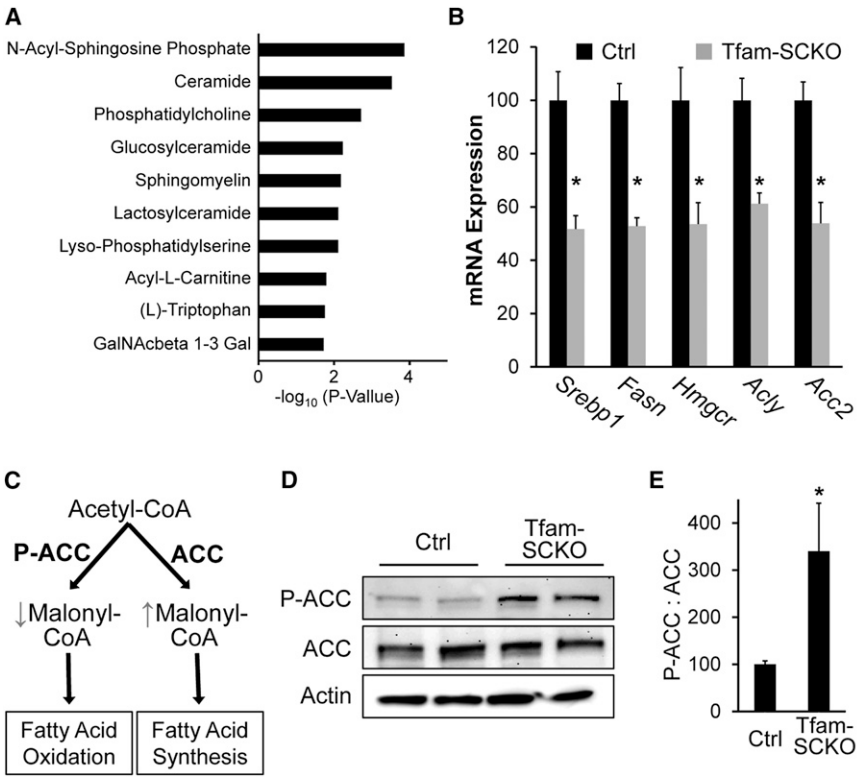

Figure 4. SC Mitochondrial Dysfunction Causes a Shift in Lipid Metabolism away from Lipid Biosynthesis and toward Fatty Acid Oxidation

(A) Differentially expressed mRNAs in 2-month-old Tfam-SCKO nerves as determined by microarray analysis are enriched for genes involved in lipid metabolism pathways. The ten pathways with the most significant enrichment among differentially expressed genes in Tfam-SCKO nerves are shown.

(B) qRT-PCR analysis confirms that a number of lipid-synthesis-related enzymes are downregulated in 2-month-old Tfam-SCKO versus Ctrl nerves. *Srebp1*, sterol regulatory element binding transcription factor 1; *Acly*, ATP citrate lyase; *Acc2*, ACC beta (primarily localized to mitochondria). N = 5 mice per genotype. Error bars represent SEM; *p < 0.05.

(C) Diagram depicting the regulation by ACC of the balance between fatty acid synthesis and oxidation, and how it is altered by ACC's phosphorylation status.

(D and E) Immunoblot analysis (D) and quantification of band intensity (E) show increased phosphorylation of ACC in 2-month-old Tfam-SCKO nerves. Phosphorylation inhibits this central regulator of the balance between lipid synthesis and oxidation, indicating (together with gene-expression results) a shift in lipid metabolism away from new lipid synthesis and toward increased lipid oxidation in SC following mitochondrial dysfunction. N = 4 mice per genotype. Error bars represent SEM; *p < 0.05.

See also Table S1.

away from lipid synthesis toward oxidation following SC mitochondrial deficits (Figure 4).

The severity of the AC buildup in 2-month-old Tfam-SCKO nerves, however, indicates that the increased shunting of lipids toward β-oxidation was accompanied by a decrease in the ability of SCs to oxidize them. The large presence of hydroxy-ACs (Figure S3E) and the reduced NAD^+/NADH ratio in Tfam-SCKO nerves (Figure S3F) indeed suggest the inhibition of the rate-determining step in β-oxidation of fatty acids. This step is catalyzed by 3-hydroxyacyl CoA dehydrogenase, which converts β-hydroxy-acyl-CoA to keto-acyl-CoA (Figure 6C). Inhibition of this NAD^+-dependent step of β-oxidation (by a decreased NAD^+/NADH ratio) leads to accumulation of the transient intermediate 3-hydroxy-acyl-CoA, which can then be converted to hydroxy-ACs (Su et al., 2005).

Note that although the buildup of ACs peaked at 2 months of age in Tam-SCKO mice, it was already detectable at 1 month of age (total AC content nmol/mg, Ctrl = 0.58 ± 0.01, Tfam-SCKO = 2.41 ± 0.22, p > 0.01; Figures S3A and S3B). AC accumulation thus preceded all other lipid abnormalities in Tfam-SCKO nerves and its increase coincided with worsening axonal pathology in these mice. This timing, together with evidence that high levels of ACs can be toxic, indicates that accumulation of ACs in Tfam-SCKO nerves is a likely contributor to the neuropathy present in these mice. In fact, genetic diseases that inhibit fatty acid β-oxidation and lead to accumulation of ACs often present with severe forms of peripheral neuropathy (Schaefer et al., 1996; Tyni and Pihko, 1999).

ACs Can Be Released from SCs and Cause Axonal Toxicity

Given the dramatic increase in AC concentration in Tfam-SCKO nerves, we examined the possibility that ACs cause the axonal degeneration observed in Tfam-SCKO mice. This amphiphilic metabolite adversely alters the properties of membranes and ion channels with devastating effects (Yamada et al., 2000). Since ACs can cross the plasma membrane (Houten and Wanders, 2010) and SCs are intimately associated with axons in peripheral nerves, we hypothesized that release of ACs from SCs onto the surrounding axons could alter axonal membrane properties and ion homeostasis, and contribute to the severe axon degeneration phenotype in Tfam-SCKO nerves as well as in neuropathies that present with prominent axonal loss.

To test this hypothesis, we first examined whether long-chain ACs are released from SCs onto surrounding axons. Two-month-old Ctrl and Tfam-SCKO nerves were cultured as explants for 2.5 days. At the end of this time, we measured the amount of long-chain ACs released from the nerves into the culture media. Whereas Ctrl nerves released very low levels of long-chain ACs into the surrounding media, Tfam-SCKO nerves secreted 35-fold more long-chain ACs (primarily C16 and C18; Figure 6D). Remarkably, the buildup of long-chain ACs from

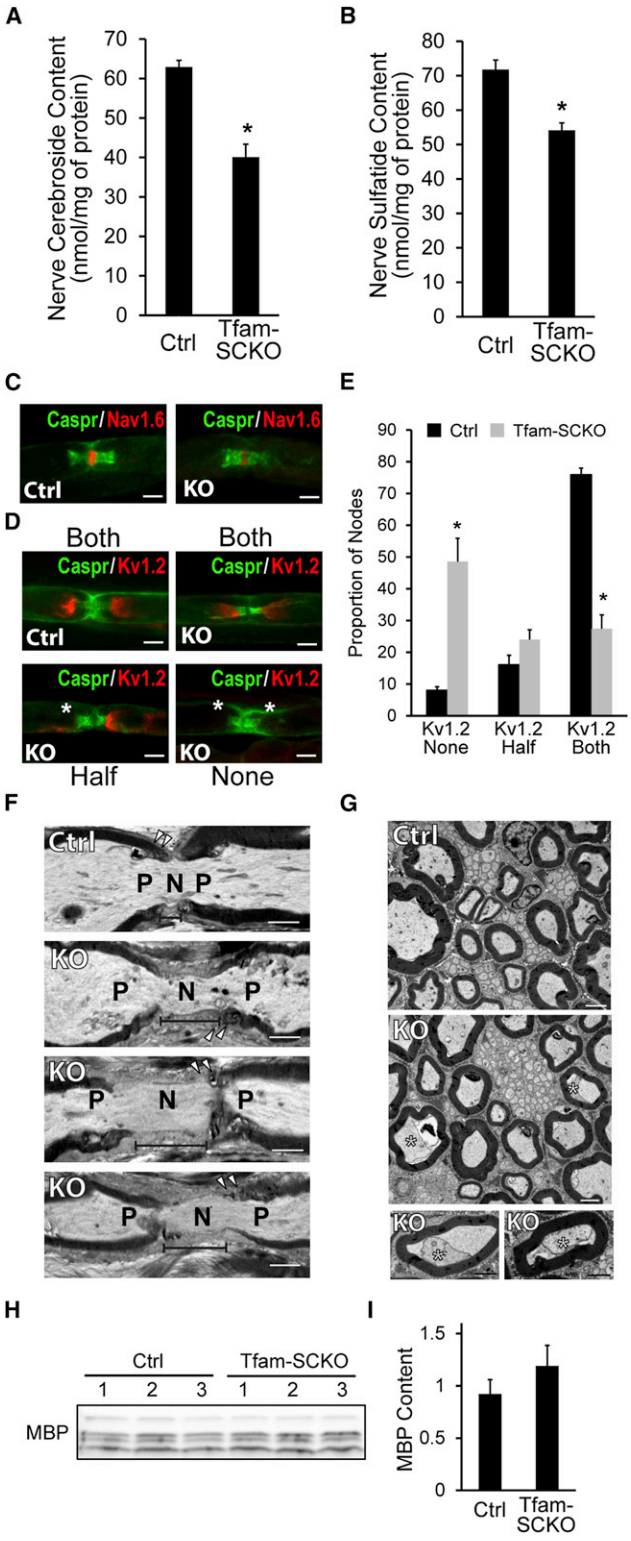

Figure 5. Abnormal Lipid Metabolism Secondary to Mitochondrial Dysfunction Results in Depletion of Myelin Lipid Components and Disrupts Axon–SC Interactions in Tfam-SCKO Nerves

(A and B) Lipidomic analysis reveals an early and significant depletion of two key myelin lipid components, CBs (A) and STs (B), in 2-month-old Tfam-SCKO versus Ctrl nerves. N = 5 mice per genotype. Error bars represent SEM; *$p < 0.05$.

(C and D) Immunostaining of nodal architecture in 2-month-old Ctrl and Tfam-SCKO nerves with antibodies against nodal (Nav1.6; C), paranodal (Caspr; C and D), and juxtaparanodal (Kv1.2; D) markers shows normal clustering of voltage-gated sodium channels (Nav1.6; C) but aberrant localization or loss of voltage-gated potassium channel clusters (Kv1.2; D) around a significant number of nodes following CB and ST depletion. Asterisks mark missing Kv1.2 clusters (D). Scale bar, 50 μm.

(E) Quantification of the number of nodes in 2-month-old Ctrl and Tfam-SCKO nerves with intact Kv1.2 clusters (both) or with missing Kv1.2 clusters at either one (half) or both sides of the node (none) as visualized in (D) confirms disruption of ion channel clustering in Tfam-SCKO versus Ctrl nerves following reductions in myelin-lipid components. N = 3 mice per genotype at each age. Error bars represent SEM; *$p < 0.05$.

(F) Longitudinal electron micrographs from 2-month-old Tfam-SCKO sciatic nerves show enlarged nodal gaps compared with Ctrls (segment line), indicating abnormal axo-glial contacts around the nodes of Ranvier. N, node; P, paranode; arrowheads, paranodal loops. Scale bar, 2 μm.

(G) Cross-sectional electron micrographs from 2-month-old Tfam-SCKO sciatic nerves display a significant number of axons that have pulled away from their myelin ensheathments (asterisks) compared with Ctrls, indicating disrupted axo-glial adhesion in Tfam-SCKOs following CB and ST depletion. Scale bar, 2 μm.

(H and I) Immunoblot analysis (H) and quantification (I) of 2-month-old nerves reveal that ST and CB depletion precedes any decrease in expression of nerve MBP, making lipid depletion a potential driver of the later demyelination. N = 3 mice per genotype. Error bars represent SEM.

See also Figure S2.

a single Tfam-SCKO nerve in 100 μl of media reached up to ≈2 μM within 2.5 days.

We next assessed the ability of ACs to disrupt axonal membrane properties and ion homeostasis. We specifically focused on the effect of ACs on axonal calcium levels (Ca^{2+}) because long-chain ACs have been shown to alter Ca^{2+} homeostasis in cardiac muscle (Yamada et al., 2000). Ca^{2+} is also important for axonal integrity and function: intra-axonal Ca^{2+} elevation often leads to severe axon degeneration (George et al., 1995), and its homeostasis is disrupted in peripheral neuropathies (Fernyhough et al., 2010). Acute application of palmitoyl-carnitine (PC), one of the most highly increased AC species in Tfam-SCKO nerves, caused a significant elevation of intracellular Ca^{2+} in cultured dorsal root ganglion (DRG) neurons loaded with the calcium dye Fluo-4 (Figures 6E and 6F). This rise in intracellular Ca^{2+} took place within minutes after exposure to AC, was dose dependent, and was specific to ACs; application of the corresponding free fatty acid at the same concentrations exerted no comparable effect (Figures 6E and 6F). The acute influx of Ca^{2+} after addition of PC also caused significant axonal blebbing (Figures 6E and 6G), which when severe enough results in axonal degeneration.

Finally, we explored the long-term effect of chronic exposure to moderate levels of ACs on axonal stability, because this more likely recapitulates the situation in vivo. For these experiments, we applied 25 μM PC onto DRG neurons daily for up to 9 days. This concentration caused no immediate axonal degeneration when applied acutely and was close to the range of long-chain ACs released from a single Tfam-SCKO nerve cultured as an explant (Figure 6D). Interestingly, the axons were able to withstand exposure to 25 μM PC for up to 4 days. After

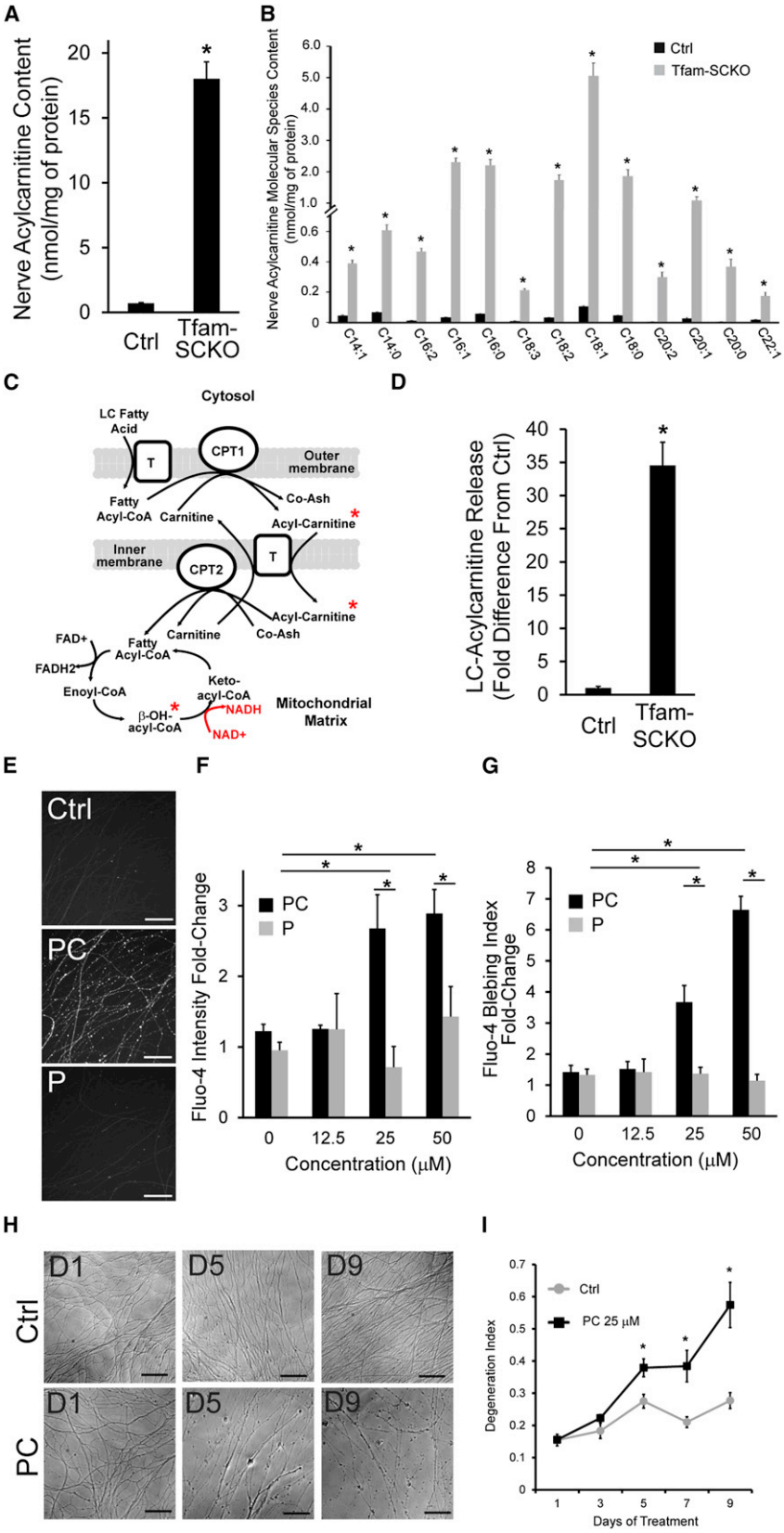

Figure 6. SC Accumulation and Release of AC Fatty Acid β-Oxidation Intermediates Secondary to Mitochondrial Dysfunction Disrupts Axonal Calcium Homeostasis and Stability

(A and B) Lipidomic analysis shows a significant accumulation of long-chain ACs (total; A) that affects most long-chain molecular species (B) in 2-month-old Tfam-SCKO versus Ctrl nerves. N = 5 mice per genotype. Error bars represent SEM; *p < 0.05.

(C) Diagram depicting fatty acid β-oxidation in the mitochondria. Long-chain fatty acids are converted to ACs to be shuttled into the mitochondrial matrix, the site of β-oxidation, where they are oxidized through repeated cycles of four enzymatic reactions. Red text indicates the altered ratio of NAD/NADH$^+$ in Tfam-SCKO nerves. Red stars indicate lipid intermediates accumulating in Tfam-SCKO nerves following mitochondrial dysfunction. Cpt1 and Cpt2, carnitine palmitoyltransferase 1 and 2; T outer, long-chain fatty acid transporter; T inner, carnitine-AC translocase; Co-Ash, coenzyme A.

(D) Explanted 2-month-old Tfam-SCKO nerves, but not Ctrl nerves, release long-chain ACs into surrounding culture media as measured by mass spectrometry. N = 6 mice per genotype. Error bars represent SEM; *p < 0.05.

(E) Images depicting increased fluorescence intensity of the Ca^{2+} dye Fluo-4 after acute (30 min) application of PC, an AC species that is highly increased in Tfam-SCKO nerves, shows that this lipid intermediate can disrupt axonal calcium homeostasis. Note that similar changes were not seen when the corresponding free fatty acid (palmitate [P]) was applied. Scale bar, 100 μm.

(F and G) Quantification of the effect of PC on Fluo-4 intensity (F) and Ca^{2+} blebbing (G) shows that the effect of this lipid intermediate on axonal calcium is dose dependent and specific to ACs; application of the corresponding free fatty acid at the same concentrations exerted no comparable effect. N = triplicate wells from one out of three representative experiments. Error bars represent SEM; *p < 0.05.

(H) Images depicting a progressive increase in axonal degeneration following chronic application of 25 μM PC for 9 days. Scale bar, 100 μm.

(I) Quantification of axonal degeneration after chronic treatment with 25 μM PC shows a significant, progressive increase in the axon degeneration index. N = 3 independent experiments with four to six wells per condition. Error bars represent SEM; *p < 0.05.

See also Figure S3.

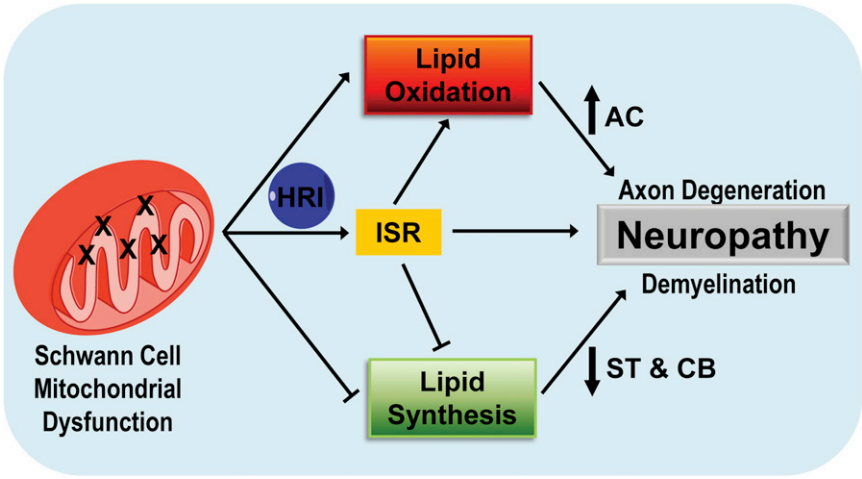

Figure 7. Altered SC Lipid Metabolism Accompanied by the Toxic Accumulation of Lipid Intermediates Induces Axonal Degeneration and Demyelination in Mitochondria-Related Peripheral Neuropathies

Diagram describing the proposed model for how activation of a maladaptive ISR as well as a shift in lipid metabolism away from lipid synthesis and toward lipid oxidation secondary to SC mitochondrial dysfunction may contribute to pathology in peripheral neuropathies.

4 days, however, prominent axonal blebbing started to develop, and axonal degeneration followed soon thereafter and progressively worsened (Figures 6H and 6I). These results demonstrate that the long-chain ACs that accumulate in SCs following mitochondrial dysfunction can be released out of these glia onto the surrounding axons. Moreover, exposure of axons to long-chain ACs can disrupt axonal membrane properties and ion homeostasis, compromising axonal stability over time. Together, our findings suggest that depletion of myelin lipid components and accumulation of toxic lipid intermediates in SCs with dysfunctional mitochondria are underlying pathological mechanisms in peripheral neuropathies.

DISCUSSION

In this study we used a recently developed mouse model (Viader et al., 2011) to identify the main disease processes in SCs that contribute to the pathology of mitochondria-related peripheral neuropathies. We show that respiratory-chain deficiency in SCs activates a maladaptive ISR through the phosphorylation of eIF2α by HRI kinase. Moreover, we demonstrate that mitochondrial dysfunction induces the remodeling of SC lipid metabolism away from synthesis and toward oxidation. This shift in lipid metabolism results in the depletion of important lipid myelin components, which initially disrupts axo-glial interactions and is a likely driver of subsequent demyelination in mitochondria-related neuropathies. Finally, we propose a mechanism by which lipid abnormalities in SCs can exacerbate axonal loss in peripheral neuropathies through the release of toxic long-chain ACs (Figure 7). Activation of a maladaptive ISR and disruption of SC lipid metabolism homeostasis secondary to mitochondrial dysfunction are thus critical underlying pathological mechanisms in peripheral neuropathies.

Mitochondrial dysfunction is a common cause of peripheral neuropathies. We recently generated the first mouse model (Tfam-SCKOs) that is useful for directly interrogating the contribution of SC mitochondrial derangements to peripheral neuropathy by disrupting mitochondria specifically in these glia (Viader et al., 2011). Interestingly, SC mitochondrial deficits in Tfam-SCKO mice did not affect the survival of these glia, and instead resulted in a severe, progressive neuropathy characterized by extensive axonal degeneration that recapitulated critical features of human peripheral nerve diseases (Viader et al., 2011). These results showed that normal mitochondrial function in SCs is essential for maintaining the axo-glial interactions that are required for long-term support of axons and normal peripheral nerve function. Moreover, our study demonstrates that SC mitochondria are underappreciated contributors to the abnormalities observed in neuropathies, since key pathological features commonly encountered in human peripheral nerve disease could be explained by SC-specific mitochondrial dysfunction. Therefore, investigators seeking to develop effective therapies for peripheral neuropathies will need to address the mechanisms by which SCs contribute to disease progression, and, as shown above, Tfam-SCKO mice could be particularly useful in this undertaking.

Our examination of Tfam-SCKO mice uncovered the activation of the ISR in Tfam-deficient SCs secondary to mitochondrial dysfunction. The ISR is a conserved, stress-activated gene-expression program centered on phosphorylation of eIF2α (Dalton et al., 2012). Activation of this program is meant to promote a cellular stress-resistant state by global attenuation of protein synthesis, which reduces the ER load and diverts amino acids from energetically costly protein synthesis to other metabolic pathways (Walter and Ron, 2011). Activation of the ISR in SCs, however, has previously been shown to be particularly maladaptive. In a model of CMT caused by mutations to myelin P_0, accumulation of mutant P_0 in the ER activated the ISR as part of a UPR (Pennuto et al., 2008). Importantly, blocking the induction of this pathway prevented the behavioral and pathological presentations of this disease model. This and other studies led to the notion that UPR-mediated activation of the ISR in SCs contributes to the pathology in myelin-related neuropathies (Lin and Popko, 2009). Here, we show that defects in mitochondrial respiration can also induce eIF2α phosphorylation and ISR through the actions of HRI kinase independently of ER stress. The maladaptive activation of the ISR in SCs through distinct eIF2α kinases that respond to diverse stressors (e.g., HRI to mitochondrial dysfunction, and PERK to ER stress) may thus be a central pathological mechanism common to diverse forms of neuropathy. This is highlighted by the fact that chemotherapeutic agents that cause neuropathy also activate the ISR in cultured cells (Gately et al., 1996).

The experiments described above also revealed a dramatic remodeling of SC lipid metabolism away from synthesis and toward oxidation following mitochondrial deficits. Lipids play a crucial role in the normal biology of SCs (Chrast et al., 2011), and the observed early shift in the lipid metabolism of Tfam-SCKO nerves is likely to participate in the subsequent neuropathy phenotype of these mice. The depletion of CBs and STs from Tfam-deficient SCs, which together represent almost 30% of all myelin lipid content (Garbay et al., 2000), could account for the prominent demyelinating phenotype apparent in late stages of disease in Tfam-SCKO mice (Figure 1; Viader et al., 2011). Moreover, given the central role of STs and CBs in maintaining axon-supportive axon–glia contacts (Figure 5; Dupree et al., 1998; Hoshi et al., 2007), their depletion could also drive some of the axon loss in Tfam-SCKO nerves. This axonal degeneration is likely exacerbated by the accumulation of ACs in Tfam-SCKO nerves following mitochondrial dysfunction. Accordingly, long-chain ACs accumulating in SCs could be released onto surrounding axons, where they could disrupt axon membrane properties and induce axon degeneration (Figure 6). These results are consistent with presentations of peripheral neuropathy in patients with genetic defects in fatty acid β-oxidation that lead to a buildup of ACs (Schaefer et al., 1996; Tyni and Pihko, 1999). Together, our results suggest that alterations in SC lipid metabolism, particularly defects in β-oxidation, may be central pathological mechanisms of mitochondrial-related neuropathies.

Interestingly, although the precise downstream cellular processes initiated by the ISR that are maladaptive to SCs are unclear, recent reports have linked activation of this pathway to altered lipid metabolism. ISR induction is reported to decrease expression of lipid biosynthetic genes (Harding et al., 2005), alter intermediate lipid metabolism (Oyadomari et al., 2008), and cause an overall shift away from lipogenesis and toward oxidation (Qi et al., 2006). The results described above are consistent with a decreased shunting of fatty acids toward new lipid synthesis and a concomitant increase in fatty acid oxidation in the nerves of Tfam-SCKO mice. The pathological remodeling of SC lipid metabolism in Tfam-SCKO mice could thus be mediated, at least in part, by the maladaptive HRI-dependent activation of the ISR following respiratory-chain deficiency in SC mitochondria. The interaction between these two main neuropathy-driving processes in Tfam-SCKO nerves highlights their potential as therapeutic targets. Moreover, it suggests that the pathological lipid metabolic abnormalities identified here in the context of SC mitochondrial deficits could be relevant to a number of other neuropathies and encephalopathies that present with ISR activation, such as CMT disease, Pelizaeus-Merzbacher disease, vanishing white matter disease, and multiple sclerosis (Lin and Popko, 2009).

Metabolic support of axons by ensheathing cells has been postulated to be critical to the ability of both central (oligodendrocytes [OLs]) and peripheral (SCs) glia to maintain axonal stability and function (Nave and Trapp, 2008). For example, SCs and OLs could support axons through the transfer of metabolites, as is the case for CNS neurons and astrocytes (Benarroch, 2005). A recent report (Fünfschilling et al., 2012) showed that mitochondrial deficits in OLs provoked an increased reliance on glycolysis by these glia to meet their energy requirements. Since these mice did not develop encephalopathy, the glycolytic shift presumably preserved oligodendrocyte viability as well as their ability to generate the metabolic intermediates necessary to support ensheathed axons. Following mitochondrial dysfunction in Tfam-SCKOs, we observed similar metabolic adaptations in SCs, which helped maintain their cellular energy levels and ensure their long-term survival (Figures 1 and S1; Viader et al., 2011). In the case of SCs, however, increased glycolysis and residual mitochondrial function were apparently insufficient for preservation of peripheral axons. These results suggest that activation of maladaptive cellular pathways and generation of toxic lipid species rather than loss of metabolic support may ultimately account for much of the SC-mediated pathology observed in mitochondria-related peripheral neuropathies.

In summary, the use of Tfam-SCKO mice, a model of neuropathy secondary to mitochondrial dysfunction, enabled us to examine the mechanisms by which deficits in mitochondrial metabolism in SCs specifically contribute to peripheral nerve diseases. Our work demonstrates that mitochondrial deficits activate a maladaptive stress response in SCs and cause a shift in the lipid metabolism of these glial cells. We provide evidence that the resulting early depletion of important lipid myelin components, as well as the accumulation and release of toxic lipid intermediates from SCs, drives the pathology observed in Tfam-SCKO mice. New therapeutic strategies that prevent depletion of lipids that support axo-glial interactions and block accumulation of fatty acid intermediates with marked axonal toxicity may be useful for treating patients with diabetic neuropathy and other mitochondria-related peripheral nerve disorders.

EXPERIMENTAL PROCEDURES

Mating of Transgenic Animals

All animal experiments were carried out in compliance with institutional animal protocols. Tfam-SCKO mice (P_0-Cre$^{-/+}$, *Tfam*$^{loxP/loxP}$) and Ctrl littermates (P_0-Cre$^{-/-}$, *Tfam*$^{loxP/loxP}$) were generated by crossing Tfam$^{loxP/loxP}$ mice (Larsson et al., 1998) to P_0-Cre mice (Feltri et al., 1999). Mating and genotyping were carried out as previously described (Viader et al., 2011).

Nerve Histology and Morphometry

For nerve histology and morphometry, sciatic nerves from Ctrl and Tfam-SCKO mice of different ages were embedded in 100% epoxy. Sections (1 μm thick) were prepared and stained with toluidine blue for light microscopy, and ultrathin sections (100 nm thick) were prepared for electron microscopy. All of the nerves underwent qualitative assessment of neural architecture followed by detailed histomorphometric analysis carried out as previously described (Hunter et al., 2007). Frozen sections or teased nerve fibers were used for immunohistochemical analysis of sciatic nerves. Following incubation with the appropriate primary and secondary antibodies, all slides were mounted for microscopic visualization using an upright epifluorescent microscope (Nikon 80i; CoolSnapES camera). Images were processed using MetaMorph and ImageJ (see Supplemental Experimental Procedures for details).

Metabolite Measurements

For ATP, ADP, AMP, and lactate measurements, sciatic nerves were extracted with perchloric acid and assayed by high-performance liquid chromatography. Elution peaks were compared with standards for identification and quantification, and levels were normalized to tissue weight (see Supplemental Experimental Procedures for details). EC was defined as ([ATP]+1/2[ADP])/([ATP]+[ADP]+[AMP]). Lactate levels were determined spectrophotometrically as

previously described (Marbach and Weil, 1967). NAD+, $NADH^+$, and the NAD+/NADH ratio were determined using a CycLex NAD+/NADH colorimetric assay kit (MBL International) according to the manufacturer's protocol.

Western Blotting

For western blotting, sciatic nerves were homogenized by sonication, and proteins were separated by SDS-PAGE and transferred to a polyvinylidene difluoride (PVDF) membrane (Millipore). Membranes were then blocked and incubated overnight with the appropriate primary antibody (see Supplemental Experimental Procedures for details). Following incubation with secondary antibodies conjugated to horseradish peroxidase (HRP; GE Healthcare), the membranes were developed with SuperSignal West Dura substrate (Pierce). The optical density of the signals was determined using ImageJ.

RNA Preparation and qRT-PCR

Total RNA was isolated after homogenization (for sciatic nerves) or lysis (for cultured SCs) in Qiazol lysis reagent (QIAGEN) using a miRNeasy Minikit (QIAGEN) according to the manufacturer's protocol. RNA concentration was quantified using an ND-1000 spectrophotometer (Nanodrop Technologies). mRNA was reverse transcribed from 100 ng of total RNA using qScript cDNA SuperMix (Quanta Biosciences). mRNA qRT-PCR was performed using a SYBR green-based detection system on a 7900 HT Sequence Detector instrument (Applied Biosystems) as described previously (Nagarajan et al., 2001). Glyceraldehyde-3-phosphate dehydrogenase (GAPDH) expression was used to normalize samples and obtain relative expression values that were used to calculate percent changes. See Supplemental Experimental Procedures for primer sequences.

Microarray and Computational Analysis

Total RNA samples were prepared by isolating and pooling RNA from at least three different 2-month-old Tfam-SCKO and Ctrl mice. Replicates were prepared entirely independently from two separate pools of at least three animals each, and two replicates were used. WG-6 v2.0 Expression BeadChip arrays (Illumina) were used according to the manufacturer's recommendations (see Supplemental Experimental Procedures for details). To analyze the resulting data, we performed a two-class unpaired significance analysis of microarrays (SAM) analysis. Differentially expressed genes with at least 2-fold differential regulation between Tfam-SCKO and Ctrl nerves at a false discovery rate (FDR) of 0.5% were selected for further analysis. Gene enrichment of the metabolic pathway was examined using GeneGO (Genego).

Nerve Sample Lipid Extract Preparation and Analysis by Multidimensional Mass-Spectrometry-Based Shotgun Lipidomics

Lipid extraction of nerve samples was performed essentially as described previously (Han et al., 2008). A triple-quadrupole mass spectrometer (TSQ Quantum Ultra Plus; Thermo Fisher) equipped with an automated nanospray apparatus (Nanomate HD; Advion Bioscience Ltd.) and Xcalibur system software together with building block analyses (Yang et al., 2009) were utilized to identify each individual lipid species in a lipid class (see Supplemental Experimental Procedures for details).

Primary SC Cultures and In Vitro ISR Induction

Primary rat SCs were cultured from sciatic nerves of postnatal day 1–3 rat pups as previously described (Nagarajan et al., 2001). For SC in vitro ISR induction assays, SCs were initially seeded onto collagen-coated 24-well plates (~75,000 cells/well) in 10% fetal bovine serum (FBS)-Dulbecco's modified Eagle's medium (DMEM) supplemented with 2 μM forskolin and 20 μg/ml of bovine pituitary extract. The cells were switched 48 hr later to 1% FBS-DMEM for 2 days to stop proliferation. At this point, the SCs were treated with either vehicle, 5 μM CCCP, 2.5 μM oligomycin, 10 μM antimycin, or 1 μM tunicamycin. RNA and protein were isolated 24 hr later. The reported results are from duplicate wells from at least three independent assays.

eIF2α Kinase Small Hairpin RNA Knockdown in 3T3 Cells and In Vitro ISR Induction

NIH 3T3 cells were infected with lentivirus expressing small hairpin RNA (shRNA) to one of four eIF2α kinases (HRI, PKR, PERK, and GCN2; see Supplemental Experimental Procedures for details). The infected cells were selected by growth in puromycin for 5 days, and cell populations with significant knockdown of each kinase were obtained and frozen as polyclonal populations. The polyclonal populations of cells were then seeded onto 24-well plates (~50,000 cells/well) in 10% FBS-DMEM. Sixteen hours after seeding, the cells were treated with either vehicle or 5 μM CCCP for 3 hr (for p-eIF2α induction) or 6 hr (for DDIT3/CHOP induction). The cells were then harvested for western blot analysis.

AC Release Measurements

To measure the ability of Tfam-deficient SCs to secrete long-chain ACs, nerves were explanted from Tfam-SCKO and Ctrl mice and maintained in 100 μl of 10% FBS supplemented with 2 mM L-glutamine and 100 ng/ml of nerve growth factor for 2.5 days. At this time, the medium was collected and immediately frozen in liquid nitrogen. The medium was then analyzed for AC species content (C2–C18 saturated, unsaturated, and hydroxylated) as butyl esters by direct flow injection and precursor ion scanning on an API 3200 LC-MS/MS system (Applied Biosystems). Quantitation was achieved using a cocktail of internal standards. Concentrations were normalized to tissue weight.

DRG Neuron Culture and Fluo-4 Imaging

Mouse DRG neurons isolated from E12 embryos were seeded onto 24-well or 96-well cell culture plates coated with poly-D-lysine (Sigma) and laminin (Invitrogen), and all experiments were carried out 5–6 days after seeding. For calcium imaging experiments, neurons were incubated with the calcium indicator Fluo-4 AM (2 μM; Invitrogen) and neurons were then treated with vehicle, PC (Sigma), or palmitate (Sigma) at the appropriate concentrations. Phase and fluorescence images were acquired every 15 min for up to 6 hr using an Operetta imaging system equipped with an environmental chamber (Perkin Elmer), and automated image analysis was carried out using ImageJ. To examine the effect of chronic AC exposure, DRG neurons were treated daily for up to 9 days with vehicle or with PC at the appropriate concentration (see Supplemental Experimental Procedures for details).

Statistical Analysis

All values are expressed as mean ± SEM, and, if no units are specified, are expressed as percent of control. If not stated otherwise, p values were determined by unpaired, two-tailed Student's t test. All statistical analyses were performed using Microsoft Excel 2007.

ACCESSION NUMBERS

The Gene Expression Omnibus (GEO) accession number for the microarray data reported in this paper is GSE44605.

SUPPLEMENTAL INFORMATION

Supplemental Information includes three figures, one table, and Supplemental Experimental Procedures and can be found with this article online at http://dx.doi.org/10.1016/j.neuron.2013.01.012.

ACKNOWLEDGMENTS

We thank Michael A. Kiebish, Nina Pachenko, Kelli Simburger, and members of the Milbrandt laboratory for experimental assistance, comments on the manuscript, and helpful discussions; Dennis Dietzen and the St. Louis Children's Hospital Metabolic Genetics Section Core laboratory for help with AC release measurements; Nils-Goran Larsson for the *Tfam*^{loxP} mice; Lawrence Wrabetz and Albee Messing for the P_0-Cre mice; the Genome Technology Access Center (GTAC) in the Department of Genetics for help with genomic analysis; the Alvin J. Siteman Cancer Center at Washington University School of Medicine and Barnes-Jewish Hospital (St. Louis, MO) for the use of the Biomedical Informatics Core (BMC), which provided the in silico analysis service, especially Nobish Varghese. Both GTAC and BMC are partially supported by NCI Cancer Center grant P30 CA91842 to the Siteman Cancer Center and by ICTS/CTSA grant UL1RR024992 from the National Center for Research Resources, a component of the National

Institutes of Health (NIH), and NIH Roadmap for Medical Research. This work was also supported by NIH Neuroscience Blueprint Center core grant P30 NS057105 to Washington University, the HOPE Center for Neurological Disorders, National Institutes of Health Grant AG13730 (J.M.), Muscular Dystrophy Association grant 237041 (J.M.), Amyotrophic Lateral Sclerosis Foundation grant 57696 (J.M.), and PPG 2P01 HL057278 (R.W.G). R.W.G. has financial relationships with LipoSpectrum and Platomics Inc.

Accepted: January 11, 2013
Published: March 6, 2013

REFERENCES

Atkinson, D.E. (1968). The energy charge of the adenylate pool as a regulatory parameter. Interaction with feedback modifiers. Biochemistry *7*, 4030–4034.

Baloh, R.H. (2008). Mitochondrial dynamics and peripheral neuropathy. Neuroscientist *14*, 12–18.

Barber, M.C., Price, N.T., and Travers, M.T. (2005). Structure and regulation of acetyl-CoA carboxylase genes of metazoa. Biochim. Biophys. Acta *1733*, 1–28.

Barres, B.A. (2008). The mystery and magic of glia: a perspective on their roles in health and disease. Neuron *60*, 430–440.

Benarroch, E.E. (2005). Neuron-astrocyte interactions: partnership for normal function and disease in the central nervous system. Mayo Clin. Proc. *80*, 1326–1338.

Chrast, R., Saher, G., Nave, K.A., and Verheijen, M.H. (2011). Lipid metabolism in myelinating glial cells: lessons from human inherited disorders and mouse models. J. Lipid Res. *52*, 419–434.

Dalton, L.E., Healey, E., Irving, J., and Marciniak, S.J. (2012). Phosphoproteins in stress-induced disease. Prog. Mol. Biol. Transl. Sci. *106*, 189–221.

Dupree, J.L., Coetzee, T., Suzuki, K., and Popko, B. (1998). Myelin abnormalities in mice deficient in galactocerebroside and sulfatide. J. Neurocytol. *27*, 649–659.

Ekstrand, M.I., Falkenberg, M., Rantanen, A., Park, C.B., Gaspari, M., Hultenby, K., Rustin, P., Gustafsson, C.M., and Larsson, N.G. (2004). Mitochondrial transcription factor A regulates mtDNA copy number in mammals. Hum. Mol. Genet. *13*, 935–944.

Feltri, M.L., D'Antonio, M., Previtali, S., Fasolini, M., Messing, A., and Wrabetz, L. (1999). P0-Cre transgenic mice for inactivation of adhesion molecules in Schwann cells. Ann. N Y Acad. Sci. *883*, 116–123.

Fernyhough, P., Roy Chowdhury, S.K., and Schmidt, R.E. (2010). Mitochondrial stress and the pathogenesis of diabetic neuropathy. Expert Rev. Endocrinol. Metab. *5*, 39–49.

Fünfschilling, U., Supplie, L.M., Mahad, D., Boretius, S., Saab, A.S., Edgar, J., Brinkmann, B.G., Kassmann, C.M., Tzvetanova, I.D., Möbius, W., et al. (2012). Glycolytic oligodendrocytes maintain myelin and long-term axonal integrity. Nature *485*, 517–521.

Garbay, B., Heape, A.M., Sargueil, F., and Cassagne, C. (2000). Myelin synthesis in the peripheral nervous system. Prog. Neurobiol. *61*, 267–304.

Gately, D.P., Sharma, A., Christen, R.D., and Howell, S.B. (1996). Cisplatin and taxol activate different signal pathways regulating cellular injury-induced expression of GADD153. Br. J. Cancer *73*, 18–23.

George, E.B., Glass, J.D., and Griffin, J.W. (1995). Axotomy-induced axonal degeneration is mediated by calcium influx through ion-specific channels. J. Neurosci. *15*, 6445–6452.

Han, X., Yang, K., and Gross, R.W. (2008). Microfluidics-based electrospray ionization enhances the intrasource separation of lipid classes and extends identification of individual molecular species through multi-dimensional mass spectrometry: development of an automated high-throughput platform for shotgun lipidomics. Rapid Commun. Mass Spectrom. *22*, 2115–2124.

Hardie, D.G., Ross, F.A., and Hawley, S.A. (2012). AMPK: a nutrient and energy sensor that maintains energy homeostasis. Nat. Rev. Mol. Cell Biol. *13*, 251–262.

Harding, H.P., Zhang, Y., Khersonsky, S., Marciniak, S., Scheuner, D., Kaufman, R.J., Javitt, N., Chang, Y.T., and Ron, D. (2005). Bioactive small molecules reveal antagonism between the integrated stress response and sterol-regulated gene expression. Cell Metab. *2*, 361–371.

Hoshi, T., Suzuki, A., Hayashi, S., Tohyama, K., Hayashi, A., Yamaguchi, Y., Takeuchi, K., and Baba, H. (2007). Nodal protrusions, increased Schmidt-Lanterman incisures, and paranodal disorganization are characteristic features of sulfatide-deficient peripheral nerves. Glia *55*, 584–594.

Houten, S.M., and Wanders, R.J. (2010). A general introduction to the biochemistry of mitochondrial fatty acid β-oxidation. J. Inherit. Metab. Dis. *33*, 469–477.

Hunter, D.A., Moradzadeh, A., Whitlock, E.L., Brenner, M.J., Myckatyn, T.M., Wei, C.H., Tung, T.H., and Mackinnon, S.E. (2007). Binary imaging analysis for comprehensive quantitative histomorphometry of peripheral nerve. J. Neurosci. Methods *166*, 116–124.

Ilieva, H., Polymenidou, M., and Cleveland, D.W. (2009). Non-cell autonomous toxicity in neurodegenerative disorders: ALS and beyond. J. Cell Biol. *187*, 761–772.

Kalichman, M.W., Powell, H.C., and Mizisin, A.P. (1998). Reactive, degenerative, and proliferative Schwann cell responses in experimental galactose and human diabetic neuropathy. Acta Neuropathol. *95*, 47–56.

Kennedy, W.R., Wendelschafer-Crabb, G., and Johnson, T. (1996). Quantitation of epidermal nerves in diabetic neuropathy. Neurology *47*, 1042–1048.

Larsson, N.G., Wang, J., Wilhelmsson, H., Oldfors, A., Rustin, P., Lewandoski, M., Barsh, G.S., and Clayton, D.A. (1998). Mitochondrial transcription factor A is necessary for mtDNA maintenance and embryogenesis in mice. Nat. Genet. *18*, 231–236.

Lin, W., and Popko, B. (2009). Endoplasmic reticulum stress in disorders of myelinating cells. Nat. Neurosci. *12*, 379–385.

Marbach, E.P., and Weil, M.H. (1967). Rapid enzymatic measurement of blood lactate and pyruvate. Use and significance of metaphosphoric acid as a common precipitant. Clin. Chem. *13*, 314–325.

Nagarajan, R., Svaren, J., Le, N., Araki, T., Watson, M., and Milbrandt, J. (2001). EGR2 mutations in inherited neuropathies dominant-negatively inhibit myelin gene expression. Neuron *30*, 355–368.

Nave, K.A., and Trapp, B.D. (2008). Axon-glial signaling and the glial support of axon function. Annu. Rev. Neurosci. *31*, 535–561.

Niemann, A., Berger, P., and Suter, U. (2006). Pathomechanisms of mutant proteins in Charcot-Marie-Tooth disease. Neuromolecular Med. *8*, 217–242.

Oyadomari, S., Harding, H.P., Zhang, Y., Oyadomari, M., and Ron, D. (2008). Dephosphorylation of translation initiation factor 2alpha enhances glucose tolerance and attenuates hepatosteatosis in mice. Cell Metab. *7*, 520–532.

Pennuto, M., Tinelli, E., Malaguti, M., Del Carro, U., D'Antonio, M., Ron, D., Quattrini, A., Feltri, M.L., and Wrabetz, L. (2008). Ablation of the UPR-mediator CHOP restores motor function and reduces demyelination in Charcot-Marie-Tooth 1B mice. Neuron *57*, 393–405.

Qi, L., Heredia, J.E., Altarejos, J.Y., Screaton, R., Goebel, N., Niessen, S., Macleod, I.X., Liew, C.W., Kulkarni, R.N., Bain, J., et al. (2006). TRB3 links the E3 ubiquitin ligase COP1 to lipid metabolism. Science *312*, 1763–1766.

Schaefer, J., Jackson, S., Dick, D.J., and Turnbull, D.M. (1996). Trifunctional enzyme deficiency: adult presentation of a usually fatal beta-oxidation defect. Ann. Neurol. *40*, 597–602.

Schröder, J.M. (1993). Neuropathy associated with mitochondrial disorders. Brain Pathol. *3*, 177–190.

Silva, J.P., Köhler, M., Graff, C., Oldfors, A., Magnuson, M.A., Berggren, P.O., and Larsson, N.G. (2000). Impaired insulin secretion and beta-cell loss in tissue-specific knockout mice with mitochondrial diabetes. Nat. Genet. *26*, 336–340.

Su, X., Han, X., Mancuso, D.J., Abendschein, D.R., and Gross, R.W. (2005). Accumulation of long-chain acylcarnitine and 3-hydroxy acylcarnitine molecular species in diabetic myocardium: identification of alterations in

mitochondrial fatty acid processing in diabetic myocardium by shotgun lipidomics. Biochemistry *44*, 5234–5245.

Tyni, T., and Pihko, H. (1999). Long-chain 3-hydroxyacyl-CoA dehydrogenase deficiency. Acta Paediatr. *88*, 237–245.

Viader, A., Golden, J.P., Baloh, R.H., Schmidt, R.E., Hunter, D.A., and Milbrandt, J. (2011). Schwann cell mitochondrial metabolism supports long-term axonal survival and peripheral nerve function. J. Neurosci. *31*, 10128–10140.

Walter, P., and Ron, D. (2011). The unfolded protein response: from stress pathway to homeostatic regulation. Science *334*, 1081–1086.

Yamada, K.A., Kanter, E.M., and Newatia, A. (2000). Long-chain acylcarnitine induces Ca2+ efflux from the sarcoplasmic reticulum. J. Cardiovasc. Pharmacol. *36*, 14–21.

Yang, K., Cheng, H., Gross, R.W., and Han, X. (2009). Automated lipid identification and quantification by multidimensional mass spectrometry-based shotgun lipidomics. Anal. Chem. *81*, 4356–4368.